

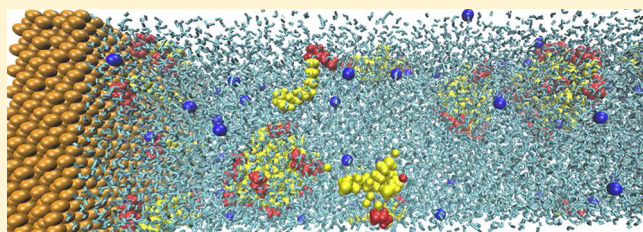
Adsorption Free Energies of Imidazolinium-Type Surfactants in Infinite Dilution and in Micellar State on Gold Surface

Yathish Kurapati and Sumit Sharma*[✉]

Department of Chemical and Biomolecular Engineering, Ohio University, Athens, Ohio 45701, United States

Supporting Information

ABSTRACT: We report adsorption behavior of imidazolinium-type surfactant molecules in different aggregation states on metal–water interfaces studied using all-atom molecular dynamics simulations. Surfactant molecules with two different alkyl tail lengths, a 10-carbon and a 17-carbon tail (henceforth referred to as imid-10 and imid-17, respectively), have been considered. Six layers of face-centered cubic lattice of gold atoms submerged in water represent the metal–water interface. Our simulations reveal that, in infinite dilution, both types of surfactant molecules strongly adsorb onto the metal–water interface in a configuration with their alkyl tail lying parallel to the surface. This adsorption occurs through a barrierless transition with an adsorption free energy of $\sim 30 k_B T$ and is found to be enthalpically driven and entropically unfavorable. Surfactant micelles, on the other hand, experience a long-range repulsion from the metal surface at distances as large as 50–60 Å due to the presence of a large “corona” around the micelles that comprises counterions and their solvation layer. Surfactant micelles have an adsorption free energy barrier of ~ 13 – $16 k_B T$, which is associated with the removal of adsorbed water from the metal surface. Micelles are thermodynamically stable in the bulk aqueous phase, and the adsorbed micellar state is only metastable.



INTRODUCTION

Adsorption of surfactants onto metal–water interfaces is useful for many applications, such as for enhancing catalytic selectivity,^{1,2} corrosion inhibition,³ tuning electrochemical properties of electrodes,^{4,5} biomimetic design,⁶ and directing growth of metal nanocrystals.⁷ Often, such applications require precise knowledge of adsorption mechanisms and adsorbed morphologies.^{1,4} The traditional viewpoint has been that the adsorption of surfactants on metal–water interfaces is driven by strong interactions between the polar head groups of the surfactants and the metal atoms.^{8–10} Furthermore, it is hypothesized that surfactants adsorb onto metal surfaces in self-assembled layers with their polar groups attached to the metal atoms.^{4,11,12} These conclusions have mainly arisen from studies of adsorption behavior from quartz crystal microbalance (QCM),¹³ saturation adsorption data,¹² electrochemical impedance spectroscopy (EIS),¹⁴ and laser scattering.¹¹ However, atomic force microscopy (AFM) experiments as well as molecular simulations suggest that the traditional picture of surfactant adsorption is imprecise on many fronts. AFM images reveal that surfactants adsorb in various morphologies, such as self-assembled monolayers (SAMs), spherical or cylindrical micelles, or hemimicelles.^{15–17} Such adsorbed morphologies have been reported in molecular simulations and are attributed to molecular geometry.¹⁸ Furthermore, there is some evidence that hydrophobic interactions between the alkyl tails play an important role in the adsorption process even for surfaces that have strong affinity for the polar head groups.^{18–20} These revelations have

important implications for practical applications. For example, to achieve electrochemical “blocking” of metal surfaces for corrosion inhibition or electrochemical reactions, an important consideration is that the surfactant molecules are able to form a tightly packed SAM.^{4,12} Therefore, choosing surfactants with appropriate geometry might be more effective rather than those with strongly polar head groups.

In an aqueous environment, surfactant molecules aggregate into micellar structures above their critical micelle concentration (CMC).²¹ Prior work on the nature of equilibrium between surfactants in micellar structures and in the adsorbed state is quite deficient. There is no consensus on whether the surfactant micelles break preceding to adsorption or the micelles themselves adsorb onto the surfaces.^{22,23} Another conundrum is the role of the adsorbed layer of water on the metal surface. Experiments performed under cryogenic conditions and in ultrahigh vacuum have established that water forms a strongly adsorbed layer over metal surfaces.²⁴ These experiments are supported by density functional theory (DFT)²⁵ as well as classical molecular simulations.²⁶ One would presume that a strongly adsorbed layer of water on metal surfaces will present a free energy barrier to adsorption, but this aspect has not been investigated so far.

Imidazolinium-type surfactants are popular corrosion inhibitors employed in the oil and gas industry.^{11,12} Figure 1 shows

Received: March 9, 2018

Revised: May 10, 2018

Published: May 11, 2018

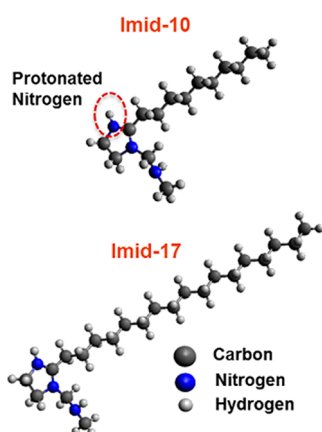


Figure 1. Structure of two imidazolium-type surfactant molecules (imid-10 and imid-17).

the chemical structure of these molecules. In oil and gas pipelines, under slightly acidic aqueous phase (pH \sim 5), the imidazolium ring of these molecules is expected to be protonated (Figure 1). In this work, we study the adsorption of imidazolium-type surfactant molecules of two different alkyl tail-lengths, a 10-carbon (imid-10) and a 17-carbon (imid-17) tail, on gold–water interface in infinite dilution and in the micellar state using all-atom molecular dynamics (MD) simulations.

METHODS

Simulation Models. The MD simulation system comprises a gold surface represented by a face-centered cubic lattice of six layers of gold atoms, protonated imidazoline-type surfactant molecules (imid-10/17), chlorides as counterions, and water molecules. We employ B3LYP level DFT with 6-31G(d,p) orbital basis sets and implicit water as solvent to calculate partial charges on atoms of protonated imid-10 and imid-17 molecules. DFT calculations are performed using the Gaussian09 software.²⁷ As expected, we do not find the partial charges on the polar headgroup to vary significantly as a function of the alkyl tail length (Table 1S and Figure 1S, Supporting Information).

Water molecules in the simulation system are represented via simple point charge enhanced (SPC/E) model.²⁸ Interaction parameters of imid-10 and imid-17 molecules are modeled using General AMBER force field (GAFF), a widely used force field for surfactants.²⁹ Chloride ions are added to the simulation system to maintain charge neutrality. Interaction parameters of chloride ions are taken from the Joung–Cheatham model.³⁰ Interaction parameters of gold atoms are taken from the interface force field developed by Heinz and co-workers.^{31,32} In the INTERFACE force field, interactions of metal atoms are modeled in the functional form of Lennard-Jones (LJ) potential. The force field parameters are derived to fit the macroscopic interfacial tension and the bulk density of metals. These force fields have been developed so that they can be coupled to AMBER or CHARMM force fields. They have been successfully employed to study the interactions between metals and organic molecules in aqueous environment.³¹

System Setup for Bulk Simulations. To study the aggregation behavior of surfactant molecules in the bulk, a three-dimensional periodic simulation box of approximate size of $90 \text{ \AA} \times 90 \text{ \AA} \times 90 \text{ \AA}$ is chosen. To generate the initial configuration, surfactant molecules, in random orientations, are

inserted at random locations in the box. This is followed by the insertion of water molecules and chloride ions. In all the insertions, overlaps between atoms are avoided. A brief (\sim 1 ns) canonical ensemble molecular dynamics (MD) simulation is performed while keeping the surfactant molecules frozen to equilibrate water and chloride. Taking the resultant configuration as the initial state, isothermal–isobaric ensemble (constant number of particles N , pressure P , and temperature T) MD simulations are performed for 6 ns in order to attain equilibrium, followed by 25–40 ns of production run at $P = 1$ bar and $T = 300$ K. Temperature and pressure are controlled by Nosé–Hoover thermostat and barostat, respectively.³³ System properties, such as total energy, pressure, radial distribution functions, and the aggregation state of surfactant molecules are monitored. Equilibrium is understood to be reached when the earlier-mentioned ensemble-averaged system properties become invariant over time.

System Setup for Simulations near Metal–Water Interface. In the cuboid-shaped simulation box of dimensions $52 \text{ \AA} \times 54 \text{ \AA} \times 190 \text{ \AA}$, six layers of gold atoms are arranged in a close-packed face-centered cubic (fcc) lattice plane (111) with the lattice constant of 4.08 \AA , parallel to the XY plane, to represent the metal surface. The simulation box is periodic in the X and Y directions and nonperiodic in the Z direction. The Z dimension is taken to be significantly larger than the X and Y dimensions to ensure that there is a sufficiently large water column representative of the bulk aqueous phase. The top three layers of metal atoms are allowed to be mobile, while the bottom three layers are kept rigid; this methodology is computationally more efficient than letting all the metal layers be mobile. Our test simulations with all the metal layers kept mobile do not show any difference in the behavior of water or surfactants in the simulation system. On the opposite face of the metal lattice in the simulation system, a \sim 5 \AA thick vapor space is maintained at the top of the aqueous phase in order to keep the system at the saturation pressure corresponding to $T = 300$ K.³⁴ The number of water molecules in the simulation box is 15,000. Spherical cutoffs of 9.8 and 14 \AA are chosen for LJ and Coulombic interactions, respectively. The particle–particle–particle mesh (PPPM) Ewald method in slab geometry is employed to account for long-range Coulombic interactions. The methodology to generate initial configurations for these simulations is the same as described earlier. Straightforward MD simulations are performed for 6 ns for attaining equilibrium, followed by 25–40 ns of production run. Equilibration is ensured by monitoring the ensemble-average system properties as described previously. All MD simulations are performed using the large-scale atomic/molecular massively parallel simulation (LAMMPS) package.³⁵

RESULTS AND DISCUSSION

Aggregation of Surfactant Molecules in Bulk. Because of their amphiphilic nature, imid-10 and imid-17 molecules have a tendency to aggregate in the bulk aqueous phase. To study this behavior, we perform a series of MD simulations in the isothermal–isobaric ensemble (NPT) wherein we systematically increase the number of surfactant molecules, N , from 2 to 64 in the simulation box. A predominantly single micelle of surfactants is formed in simulations with $N < 32$. Micelles with the number of constituent molecules, N_{micelle} , larger than 25 are not observed to form in the simulations. For instance, in the MD simulation with $N = 64$ imid-17 molecules, three micelles of average size, $N_{\text{micelle}} = 24, 19,$ and 17 , form. Excursions to

high temperatures followed by slow cooling to 300 K do not lead to coalescence of these micelles. Hence, these micelles are at least metastable. The relative stability of micelles of different sizes will be studied in a future work. To determine the shape of imid-10 and imid-17 micelles, we calculate their asphericity given by the following equation,³⁶

$$\text{asphericity} = \left[\lambda_1 - \frac{1}{2}(\lambda_2 + \lambda_3) \right] R_g^{-2} \quad (1)$$

where λ_i are principle components of the radius of gyration squared tensor with $\lambda_1 > \lambda_2 > \lambda_3$, and R_g^2 is the mean squared radius of gyration. Figure 2a shows the asphericity of micelles as

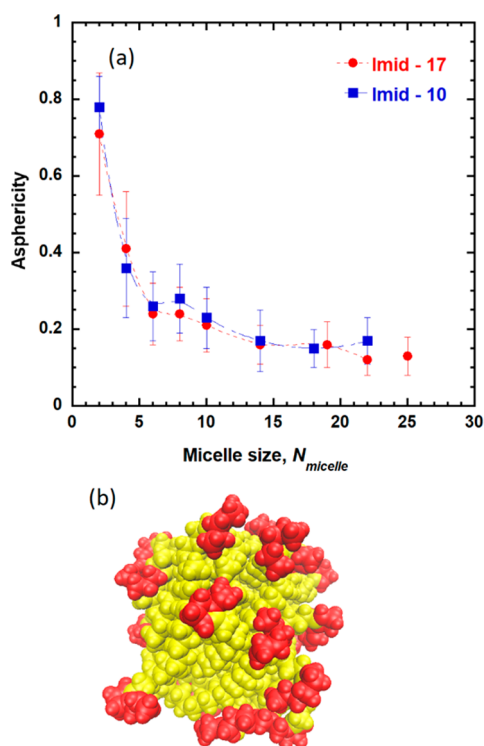


Figure 2. (a) Asphericity of micelles as a function of their size, N_{micelle} (b) Snapshot of imid-17 micelle with $N_{\text{micelle}} = 19$. Red atoms represent the imidazolium-type polar headgroup, and yellow atoms represent the atoms in the alkyl tails.

a function of their size, N_{micelle} . It is observed that, as the micelles grow in size, their asphericity becomes smaller, implying that the micelles become spherical in shape. A snapshot of an imid-17 micelle is shown in Figure 2b. It is observed that the polar head groups are predominantly exposed to water while the alkyl tails are aggregated to minimize their interactions with water.

Adsorption of Surfactants on Metal–Water Interface.

As a first step toward understanding the adsorption behavior, we introduce imid-10 and imid-17 molecules in a simulation box with six layers of gold atoms arranged in a fcc lattice parallel to one face of the simulation box (see Methods section for details of the simulation system setup). We perform canonical ensemble (NVT) simulations in the simulation box of dimensions $52 \text{ \AA} \times 54 \text{ \AA} \times 190 \text{ \AA}$ with a $\sim 5 \text{ \AA}$ vapor space on the face opposite to the metal lattice to ensure that the simulation system remains at saturation pressure. It is noted that water strongly adsorbs onto the gold surface, thereby forming two adsorbed layers (Figure 2S, Supporting

Information). In infinite dilution, the surfactant molecule adsorbs onto the metal–water interface in a “flat” configuration, that is, with its alkyl tail lying parallel to the metal surface (Figure 3S, Supporting Information). At finite concentrations, it is observed that a few (4–5 molecules out of a total of 64 surfactant molecules) molecules adsorb on the metal–water interface in the flat configuration while the remaining molecules aggregate as micelles of sizes, N_{micelle} , ranging from 17 to 24 in the bulk (Figure 4S, Supporting Information). In a 40 ns long MD simulation, these micelles are not observed to adsorb on the metal–water interface. From these set of straightforward MD simulations, it is clear that the adsorption behavior of surfactant molecules is a function of their aggregation state and deserves a closer scrutiny.

Free Energy of Adsorption of Surfactants in Infinite Dilution. To further elucidate the adsorption behavior, we calculate the free energy profiles of adsorption. For a single surfactant molecule (infinite dilution), the free energy profile is calculated by performing umbrella sampling³⁷ simulations wherein a harmonic potential is applied to the center of mass of the surfactant molecule,

$$V_i(\xi) = K(\xi - \xi_i)^2 \quad (2)$$

In the above equation, ξ is the distance along the Z-axis (that is, in the direction perpendicular to the plane of the metal layers) between the center of mass of the surfactant molecule and the center of the topmost layer of metal atoms; ξ_i is the set value of the distance for an umbrella sampling window; and K is the force constant. Overlapping umbrella sampling windows spanning distances close to the metal surface all the way up to the bulk region are generated by changing the value of ξ_i from 1 to 30 Å. In the umbrella sampling simulations, a value of ξ smaller than 3 Å is never sampled due to the excluded volume of metal atoms. For the umbrella sampling windows with $\xi_i > 9 \text{ \AA}$, the value of K is set to 21 kJ/mol. For $\xi_i < 9 \text{ \AA}$, a strong affinity of the surfactant molecule toward the metal surface is observed, and so the value of K is varied from 13 to 105 kJ/mol in different windows to ensure that efficient sampling of all values of ξ is performed. The values of K are chosen to ensure that all ξ are adequately sampled and there is sufficient overlap in the histograms of adjacent umbrella sampling windows. Figure 5S (Supporting Information) shows the histograms of different umbrella sampling windows for imid-17. Overall, we sample 51 (imid-10) and 64 (imid-17) windows. For each umbrella sampling window, we have performed simulations for 6 ns to achieve equilibrium, followed by 9 ns of simulations for the production run. The biased probability distributions obtained from different umbrella sampling simulations are stitched together to generate unbiased probability distributions using the weighted histogram analysis method (WHAM).³⁸ From these unbiased probability distributions, adsorption free energy profiles of imid-10 and imid-17 molecules in infinite dilution are obtained (Figure 3). It is observed that the surfactant molecules strongly adsorb on to the metal surface in a flat configuration with a free energy of adsorption of $\sim 30 k_B T$. A snapshot of the imid-17 molecule adsorbed in the flat configuration is shown in Figure 3S (Supporting Information). Figure 6S shows the average value of cosine of the angle between the unit vector normal to the metal surface and the unit vector joining the N1 nitrogen in the imidazolium ring (see Figure 1S to see different atom labels) and the last carbon of the alkyl tail, $\cos(\theta)$. It is observed in Figure 6S that, for $\xi < 5 \text{ \AA}$, $\cos(\theta) \approx 0$, implying that the imid-17 molecule lies flat on

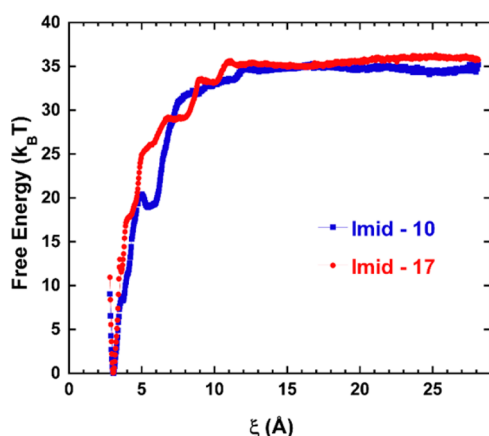


Figure 3. Adsorption free energy profiles of imid-10 and imid-17 in infinite dilution on gold surface. Free energy profiles show a barrierless adsorption for both types of molecules.

the metal surface upon adsorption. Similar behavior is observed for the imid-10 molecule as well. The calculated free energy profiles of adsorption are not smooth. This is because we do not sample the orientational space of the surfactant molecules in an exhaustive fashion. In principle, one can sample the orientational space by applying another harmonic biasing potential on the angle between the surfactant molecule and the surface normal. However, such a calculation will require at least an order of magnitude more number of simulations. In our study, we have ensured that the number of umbrella sampling simulations that we have sampled are sufficient to obtain converged free energy profiles. One interesting revelation from [Figure 3](#) is that the imid-10 and imid-17 molecules have similar adsorption free energies, that is, apparently there is no tail length dependence on the adsorption free energy. To investigate the underlying reasons for this observation, we determine the energetic and entropic components of the adsorption free energy. Because a change in the free energy profile is observed only below 10 Å, the configurations with ξ less than 10 Å are considered as adsorbed states, while the configurations with ξ greater than 10 Å are considered as bulk states. The free energy of adsorption, ΔG_{ads} , is given by

$$\Delta G_{\text{ads}} = -k_{\text{B}}T \left(\ln \left(\sum_{\xi \leq 10\text{\AA}} P^{\mu}(\xi) \right) - \ln \left(\sum_{\xi > 10\text{\AA}} P^{\mu}(\xi) \right) \right) \quad (3)$$

where $p^{\mu}(\xi)$ is the unbiased probability distribution as a function of ξ calculated from WHAM. It is important to mention here that, although we have performed canonical ensemble MD simulations, the pressure in the system is maintained constant by leaving a vapor space in the simulation box. So, the appropriate free energy of the system is the Gibbs free energy, G . The energy of adsorption is calculated as the difference between the ensemble-averaged total energy in the adsorbed and the desorbed states,

$$\Delta U_{\text{ads}} = \sum_{\xi \leq 10\text{\AA}} P^{\mu}(\xi)U(\xi) - \sum_{\xi > 10\text{\AA}} P^{\mu}(\xi)U(\xi) \quad (4)$$

where $U(\xi)$ is the total potential energy of the system in the configuration wherein the surfactant molecule is at a distance ξ . Because we observe no volume change in the aqueous phase of the simulation box between the adsorbed and the desorbed states, the $P\Delta V \approx 0$, and therefore, $\Delta U_{\text{ads}} \approx \Delta H_{\text{ads}}$. The change

in entropy due to adsorption is calculated by $\Delta S_{\text{ads}} = (\Delta H_{\text{ads}} - \Delta G_{\text{ads}})/T$. [Table 1](#) lists ΔG_{ads} , ΔH_{ads} , and ΔS_{ads} values for imid-

Table 1. Free Energy, Enthalpy, and Entropy of Adsorption of Surfactant Molecules in an Infinitely Dilute System

	imid-10	imid-17
$\Delta G_{\text{ads}} (k_{\text{B}}T)$	−30.15	−30.68
$\Delta H_{\text{ads}} (k_{\text{B}}T)$	−57.41	−75.23
$\frac{\Delta S_{\text{ads}}}{k_{\text{B}}}$	−27.26	−44.55

10 and imid-17 molecules. The energy of adsorption of imid-17 is more negative than that of imid-10, which is attributed to the favorable interactions of the longer alkyl tail of imid-17 with the metal atoms. On the other hand, the entropic loss associated with imid-17 adsorption is higher than that for imid-10, which is attributed to the loss in the conformational and translational entropy of the molecule. Hence, adsorption is energetically favored but entropically not favored.

Free Energy of Adsorption of Surfactant Micelles. To understand the adsorption behavior of surfactant micelles, we calculate the adsorption free energy of imid-10 and imid-17 micelles at the metal–water interface using umbrella sampling simulations. A micelle of size $N_{\text{micelle}} = 18$ for imid-10 and $N_{\text{micelle}} = 19$ for imid-17 is considered for this study. The rationale for selecting these micelle sizes is that these micelles are formed in our simulations, which are started with a random distribution of surfactant molecules near the metal surface. Furthermore, micelles in this size range are found to be stable in our bulk MD simulations as discussed before. These imid-10 and imid-17 micelles have root-mean-squared radius of gyration R_{g} of 11.4 and 12 Å, respectively. By considering the micelles to be uniformly distributed solid spheres, their radii can be approximated as $\sqrt{(5/3)}$ times the R_{g} , which is calculated to be ~ 15 Å. For the umbrella sampling simulations, the distance between the metal surface and the center of mass of the micelle is taken as the reaction coordinate, ξ , and the harmonic biasing potential given by [eq 2](#) is applied. The value of K is taken as 21 kJ/mol, and a total of 64 umbrella sampling windows are considered. From the umbrella sampling simulations and WHAM calculations, free energy profiles of imid-10 ([Figure 4a](#)) and imid-17 ([Figure 4b](#)) micelles are thus obtained as a function of ξ . There are two interesting features to observe in [Figure 4a](#) and [b](#): (1) unlike the infinite dilution case, there is a free energy barrier to adsorption of the micelles of magnitude 13–16 $k_{\text{B}}T$ at $\xi \approx 21$ Å; and (2) for distances as large as $\xi \approx 50$ –60 Å, the micelles experience repulsion from the metal surface. This is a surprising result as the radii of the micelles is ~ 15 Å. Hence, the repulsive interactions at distances of 50–60 Å cannot be explained simply as the interaction between the micelles and the adsorbed layers of water on the metal surface. This long-range interaction is understood when one considers the much larger “corona” around the micelles that is formed by the counterions and their solvation layer. [Figure 5a](#) shows (unnormalized) cumulative distribution of chloride ions as a function of ξ , corresponding to different center-of-mass locations of 21, 33, and 50 Å of the imid-17 micelle. That is, for any value of ξ , say ξ_0 , [Figure 5a](#) shows the number of chloride ions in the region $\xi < \xi_0$. This figure is generated by binning the locations of the chloride ions in bins of size 12 Å. The cumulative distribution of chloride ions shifts to smaller values of ξ along with the center-of-mass of the micelle,

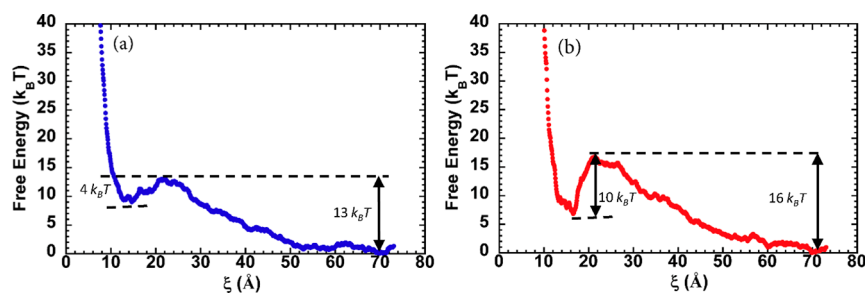


Figure 4. Adsorption free energy profiles of (a) an imid-10 micelle and (b) an imid-17 micelle on gold surface. Both micelles experience a long-ranged repulsion from the surface. The adsorbed state of the micelles is locally stable.

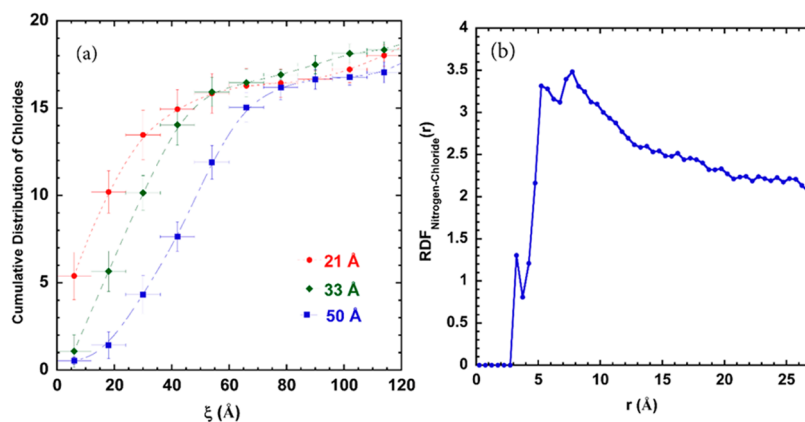


Figure 5. (a) Unnormalized cumulative distribution of chloride ions as a function of ξ for the center-of-mass locations of 21, 33, and 50 Å of the imid-17 micelle. (b) Radial distribution function between the protonated nitrogen atom of the surfactant and the chloride ions, $\text{RDF}_{\text{Nitrogen-Chloride}}(r)$ for the imid-17 micelle. In the graph, the $\text{RDF}_{\text{Nitrogen-Chloride}}(r)$ is shown only up to a distance of 25 Å, and hence it does not go to 1.

implying that the chloride ions remain in the vicinity of the micelle.

Figure 5b shows the radial distribution function of chlorides with respect to the protonated nitrogen atom in the imidazolium ring, $\text{RDF}_{\text{Nitrogen-Chloride}}(r)$. Clearly, chloride ions prefer to stay close to the protonated nitrogens, which are predominantly located on the periphery of the micelle. It should be noted that the $\text{RDF}_{\text{Nitrogen-Chloride}}(r)$ does not go to 1 in Figure 5b because we have only plotted it up to a distance of 25 Å and not for the entire simulation box. Furthermore, each chloride ion is strongly solvated, as can be seen from the radial distribution function between the chloride and the oxygen atoms of water, $\text{RDF}_{\text{Oxygen-Chloride}}(r)$ (Figure 7S, Supporting Information). Together, the counterions around the periphery of the micelle and their solvation shell form a corona of size ~ 20 Å, which interacts with the first and second layers of water adsorbed on the metal surface, giving rise to the long-range interaction observed in the free energy profiles. The peak of the free energy barrier is at $\xi \approx 21$ Å. Because the radii of the micelles are ~ 15 Å, when the micelle is at $\xi \approx 21$ Å, only a single layer of adsorbed water resides between the metal atoms and the micelle. Hence, this free energy barrier is due to the displacement of water molecules present in the first adsorbed layer on the metal surface. The imid-17 micelle is slightly larger in size as compared to the imid-10 micelle and therefore has a larger corona around it. Hence, a larger free energy barrier is observed for the case of imid-17 micelle. The minimum in the free energy profiles at $\xi \approx 15$ Å corresponds to the configuration wherein the micelle is in contact with the metal surface (Figure 6). The imid-17 micelle has a desorption free energy barrier of $\sim 10 k_B T$, whereas for the imid-10 micelle it is

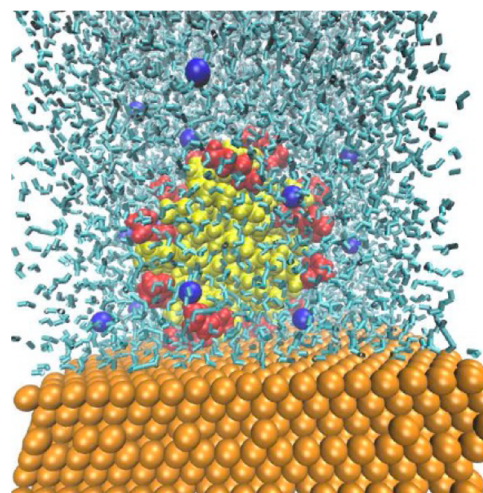


Figure 6. Snapshot taken from an unbiased simulation wherein $\xi \approx 15$ Å for an imid-17 micelle. Blue represents chlorides, yellow represents alkyl tails, red represents polar head groups, gold represents metal atoms, and cyan represents water molecules. The spherical micelle is observed to be in contact with the metal atoms.

$\sim 4 k_B T$. Because the imid-17 micelle is larger than the imid-10 micelle, it has stronger interaction with the metal atoms in the adsorbed state and, hence, has a larger desorption free energy barrier. As is noted by visualizing the micelle configurations, the increase in the free energy profile for the values of $\xi < 15$ Å is associated with the deformation of the micelles. To verify the presence of a free energy barrier at 21 Å, we study two unbiased MD trajectories: first in which initially the center of mass of the

imid-17 micelle is at $\xi > 21$ Å and the second in which the center of mass of the imid-17 micelle is at $\xi < 21$ Å. As expected, for the first trajectory, the micelle diffuses away from the metal surface, while in the second trajectory, the micelle diffuses close to the metal surface. (Figure 7). A similar observation is made for imid-10 trajectories.

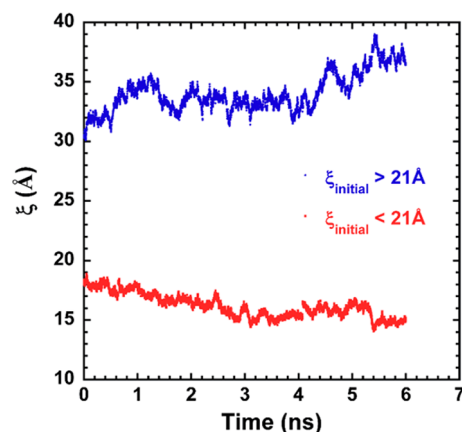


Figure 7. Two unbiased MD trajectories of an imid-17 micelle are shown with two initial positions, $\xi_{\text{initial}} = 19$ and 30 Å. The MD trajectory with $\xi_{\text{initial}} = 19$ Å diffuses toward the metal surface to reach $\xi \approx 15$ Å, which corresponds to the adsorbed state, while the MD trajectory with $\xi_{\text{initial}} = 30$ Å diffuses away from the metal.

CONCLUSIONS

In applications such as corrosion inhibition, it is important to understand the nature of dynamic equilibrium between the adsorbed and the aggregated states of surfactant molecules. Our straightforward MD simulations of imidazolium-type surfactant molecules near gold–water interfaces show that a few surfactant molecules adsorb on to the metal interface in a flat configuration, while most of the molecules aggregate rapidly in the bulk aqueous phase to form micellar structures. These micelles are not observed to adsorb on the metal surfaces in the simulation time scales. Free energy calculations reveal that, in the unaggregated state, the surfactant molecules adsorb very strongly onto metal surfaces in a barrierless transition. On the other hand, surfactants in micellar structures show a much weaker adsorption tendency. The micelles experience a long-range repulsion due to the interactions between the solvation shell of the counterions surrounding the micelles and the adsorbed layers of water on the metal surface. The surfactant micelles have a significant free energy barrier to adsorption, associated with the removal of adsorbed water molecules from the metal surface. In the adsorbed state, the micelles remain in contact with the metal atoms and do not break apart. These results suggest that, for efficient surface coverage via surfactant adsorption, one should add surfactants in concentrations below their critical micelle concentration to avoid their aggregation in the bulk phase.

ASSOCIATED CONTENT

Supporting Information

The Supporting Information is available free of charge on the ACS Publications website at DOI: 10.1021/acs.jpcc.8b02358.

Average partial charge on different atoms of protonated imidazolium-based surfactant molecule; labels of atoms

of imidazolium-based surfactant molecule; density profile of water as a function of distance from the topmost layer of gold atoms; equilibrium adsorbed state of imid-17 surfactant molecule in infinite dilution; snapshot of straightforward MD simulation of 64 imid-17 molecules near gold–water interface in the simulation system; histograms generated from umbrella sampling simulations of imid-17 molecule in infinite dilution; average values of cosine of the angle between the unit vector normal to the metal surface and the unit vector parallel to the alkyl tail of imid-17 molecule; radial distribution function of water oxygen around chloride ions (DOCX)

AUTHOR INFORMATION

Corresponding Author

*E-mail: sharmas@ohio.edu. Phone: (740) 593 1425.

ORCID

Sumit Sharma: 0000-0003-3138-5487

Notes

The authors declare no competing financial interest.

ACKNOWLEDGMENTS

The authors acknowledge the donors of the American Chemical Society Petroleum Research Fund (ACS PRF no. 56892-DNI6) for support of this research. This work is partially supported by the NSF CBET Grant 1705817. The authors thank researchers at the Institute for Corrosion and Multiphase Technology (ICMT) for useful discussions. Computational resources for this work were provided by the Ohio Supercomputer Center.

REFERENCES

- (1) Schoenbaum, C. A.; Schwartz, D. K.; Medlin, J. W. Controlling the surface environment of heterogeneous catalysts using self-assembled monolayers. *Acc. Chem. Res.* **2014**, *47*, 1438–1445.
- (2) Perez-Coronado, A. M.; Calvo, L.; Baeza, J. A.; Palomar, J.; Lefferts, L.; Rodriguez, J. J.; Gilarranz, M. A. Metal-surfactant interaction as a tool to control the catalytic selectivity of Pd catalysts. *Appl. Catal., A* **2017**, *529*, 32–39.
- (3) Finšgar, M.; Jackson, J. Application of corrosion inhibitors for steels in acidic media for the oil and gas industry: A review. *Corros. Sci.* **2014**, *86*, 17–41.
- (4) Li, J.; Kaifer, A. E. Surfactant monolayers on electrode surfaces: self-assembly of a viologen derivative having a cholesteryl hydrophobic residue. *Langmuir* **1993**, *9*, 591–596.
- (5) Vittal, R.; Gomathi, H.; Kim, K.-J. Beneficial role of surfactants in electrochemistry and in the modification of electrodes. *Adv. Colloid Interface Sci.* **2006**, *119*, 55–68.
- (6) Naik, R. R.; Stringer, S. J.; Agarwal, G.; Jones, S. E.; Stone, M. O. Biomimetic synthesis and patterning of silver nanoparticles. *Nat. Mater.* **2002**, *1*, 169–172.
- (7) Luo, M.; Ruditskiy, A.; Peng, H. C.; Tao, J.; Figueroa-Cosme, L.; He, Z.; Xia, Y. Penta-twinned copper nanorods: facile synthesis via seed-mediated growth and their tunable plasmonic properties. *Adv. Funct. Mater.* **2016**, *26*, 1209–1216.
- (8) Ramachandran, S.; Tsai, B.-L.; Blanco, M.; Chen, H.; Tang, Y.; Goddard, W. A. Self-assembled monolayer mechanism for corrosion inhibition of iron by imidazolines. *Langmuir* **1996**, *12*, 6419–6428.
- (9) Cruz, J.; Martinez, R.; Genesca, J.; Garcia-Ochoa, E. Experimental and theoretical study of 1-(2-ethylamino)-2-methylimidazole as an inhibitor of carbon steel corrosion in acid media. *J. Electroanal. Chem.* **2004**, *566*, 111–121.
- (10) Gece, G. The use of quantum chemical methods in corrosion inhibitor studies. *Corros. Sci.* **2008**, *50*, 2981–2992.

- (11) Edwards, A.; Osborne, C.; Webster, S.; Klenerman, D.; Joseph, M.; Ostovar, P.; Doyle, M. Mechanistic studies of the corrosion inhibitor oleic imidazoline. *Corros. Sci.* **1994**, *36*, 315–325.
- (12) McMahon, A. J. The mechanism of action of an oleic imidazoline based corrosion inhibitor for oilfield use. *Colloids Surf.* **1991**, *59*, 187–208.
- (13) Jevremović, I.; Singer, M.; Nešić, S.; Mišković-Stanković, V. Inhibition properties of self-assembled corrosion inhibitor talloil diethylenetriamine imidazoline for mild steel corrosion in chloride solution saturated with carbon dioxide. *Corros. Sci.* **2013**, *77*, 265–272.
- (14) Tan, Y.-J.; Bailey, S.; Kinsella, B. An investigation of the formation and destruction of corrosion inhibitor films using electrochemical impedance spectroscopy (EIS). *Corros. Sci.* **1996**, *38*, 1545–1561.
- (15) Jaschke, M.; Butt, H.-J.; Gaub, H. E.; Manne, S. Surfactant aggregates at a metal surface. *Langmuir* **1997**, *13*, 1381–1384.
- (16) Xiong, Y.; Brown, B.; Kinsella, B.; Nešić, S.; Pailleret, A. Atomic force microscopy study of the adsorption of surfactant corrosion inhibitor films. *Corrosion* **2014**, *70*, 247–260.
- (17) Sharma, B. G.; Basu, S.; Sharma, M. M. Characterization of adsorbed ionic surfactants on a mica substrate. *Langmuir* **1996**, *12*, 6506–6512.
- (18) Ko, X.; Sharma, S. Adsorption and self-assembly of surfactants on metal–water interfaces. *J. Phys. Chem. B* **2017**, *121*, 10364–10370.
- (19) Somasundaran, P.; Fuerstenau, D. W. Mechanisms of alkyl sulfonate adsorption at the alumina–water interface. *J. Phys. Chem.* **1966**, *70*, 90–96.
- (20) Fan, A.; Somasundaran, P.; Turro, N. J. Adsorption of alkyltrimethylammonium bromides on negatively charged alumina. *Langmuir* **1997**, *13*, 506–510.
- (21) Abbott, S. Surfactant science: principles and practice, Creative commons, 2015. <http://www.stevenabbott.co.uk/practical-surfactants/the-book.php> (accessed Sept 8, 2017).
- (22) Free, M. L. Understanding the effect of surfactant aggregation on corrosion inhibition of mild steel in acidic medium. *Corros. Sci.* **2002**, *44*, 2865–2870.
- (23) Colegate, D. M.; Bain, C. D. Adsorption kinetics in micellar solutions of nonionic surfactants. *Phys. Rev. Lett.* **2005**, *95*, 198302.
- (24) Carrasco, J.; Hodgson, A.; Michaelides, A. A molecular perspective of water at metal interfaces. *Nat. Mater.* **2012**, *11*, 667–674.
- (25) Haq, S.; Clay, C.; Darling, G. R.; Zimbitas, G.; Hodgson, A. Growth of intact water ice on Ru (0001) between 140 and 160 K: Experiment and density-functional theory calculations. *Phys. Rev. B: Condens. Matter Mater. Phys.* **2006**, *73*, 115414.
- (26) Limmer, D. T.; Willard, A. P.; Madden, P.; Chandler, D. Hydration of metal surfaces can be dynamically heterogeneous and hydrophobic. *Proc. Natl. Acad. Sci. U. S. A.* **2013**, *110*, 4200–4205.
- (27) Frisch, M. J.; Trucks, G. W.; Schlegel, H. B.; Scuseria, G. E.; Robb, M. A.; Cheeseman, J. R.; Scalmani, G.; Barone, V.; Mennucci, B.; Petersson, G. A., et al. *Gaussian 09*, Revision A.1; Gaussian, Inc.: Wallingford, CT, 2009.
- (28) Berendsen, H. J. C.; Grigera, J. R.; Straatsma, T. P. The missing term in effective pair potentials. *J. Phys. Chem.* **1987**, *91*, 6269–6271.
- (29) Wang, J.; Wolf, R. M.; Caldwell, J. W.; Kollman, P. A.; Case, D. A. Development and testing of a general amber force field. *J. Comput. Chem.* **2004**, *25*, 1157–1174.
- (30) Joung, I. S.; Cheatham, T. E., III Determination of alkali and halide monovalent ion parameters for use in explicitly solvated biomolecular simulations. *J. Phys. Chem. B* **2008**, *112*, 9020–9041.
- (31) Heinz, H.; Lin, T.-J.; Kishore Mishra, R.; Emami, F. S. Thermodynamically consistent force fields for the assembly of inorganic, organic, and biological nanostructures: the INTERFACE force field. *Langmuir* **2013**, *29*, 1754–1765.
- (32) Heinz, H.; Vaia, R. A.; Farmer, B. L.; Naik, R. R. Accurate simulation of surfaces and interfaces of face-centered cubic metals using 12–6 and 9–6 Lennard-Jones potentials. *J. Phys. Chem. C* **2008**, *112*, 17281–17290.
- (33) Allen, M. P.; Tildesley, D. J. *Computer Simulation of Liquids*; Oxford University Press: New York, 1989.
- (34) Patel, A. J.; Varilly, P.; Chandler, D. Fluctuations of water near extended hydrophobic and hydrophilic surfaces. *J. Phys. Chem. B* **2010**, *114*, 1632–1637.
- (35) Plimpton, S. Fast parallel algorithms for short-range molecular dynamics. *J. Comput. Phys.* **1995**, *117*, 1–19.
- (36) Arkın, H.; Janke, W. Gyration tensor based analysis of the shapes of polymer chains in an attractive spherical cage. *J. Chem. Phys.* **2013**, *138*, 054904.
- (37) Torrie, G. M.; Valleau, J. P. Nonphysical sampling distributions in Monte Carlo free-energy estimation: Umbrella sampling. *J. Comput. Phys.* **1977**, *23*, 187–199.
- (38) Kumar, S.; Rosenberg, J. M.; Bouzida, D.; Swendsen, R. H.; Kollman, P. A. The weighted histogram analysis method for free - energy calculations on biomolecules. I. The method. *J. Comput. Chem.* **1992**, *13*, 1011–1021.